AD NUMBER

AD481363

LIMITATION CHANGES

TO:

Approved for public release; distribution is unlimited.

FROM:

Distribution authorized to U.S. Gov't. agencies and their contractors; Critical Technology; 1962. Other requests shall be referred to Naval Postgraduate School, Monterey, CA 93943. This document contains export-controlled technical data.

AUTHORITY

USNPS ltr, 6 Oct 1971

UNITED STATES
NAVAL POSTGRADUATE SCHOOL

THESIS

ABSOLUTE AND RELATIVE SPECTRAL
LINE INTENSITY MEASUREMENTS
IN A PLASMA SHOCK TUBE

by

Mell A. Peterson, Jr.
and
John H. Kinert

1962

ABSOLUTE AND RELATIVE SPECTRAL LINE INTENSITY MEASUREMENTS IN A PLASMA SHOCK TUBE

* * * * *

Mell A. Peterson, Jr.

and

John H. Kinert

(6)

ABSOLUTE AND RELATIVE SPECTRAL LINE INTENSITY MEASUREMENTS IN A PLASMA SHOCK TUBE.

(9) Master's thesis,

by

(10) Mell A. Peterson, Jr.

[redacted]

John H. Kinert •

Lieutenant, United States Navy

Submitted in partial fulfillment of
the requirements for the degree of

MASTER OF SCIENCE
IN
PHYSICS

United States Naval Postgraduate School
Monterey, California

(11) 1962,

(12) 48p.

B

ABSOLUTE AND RELATIVE SPECTRAL

LINE INTENSITY MEASUREMENTS

IN A PLASMA SHOCK TUBE

by

Mell A. Peterson, Jr.

and

John H. Kinert

This work is accepted as fulfilling

the thesis requirements for the degree of

MASTER OF SCIENCE

IN

PHYSICS

from the

United States Naval Postgraduate School

Raymond F. Kelly
Faculty Advisor

Chairman
Dept. of Physics

Approved:

Academic Dean

ABSTRACT

A spectroscopic investigation of a plasma shock tube may reveal the number density and temperature of the constituents of the plasma. Such an investigation was conducted on a cylindrical fused quartz shock tube and a square, three inch aluminum shock tube ~~at the Physical Research Laboratory, Aerospace Corporation, Los Angeles, California~~ in June-July, 1961. Deuterium and hydrogen plasmas were investigated separately. General characteristics including ringing frequency and longitudinal visible shock front velocity were determined. Spectral line analysis from a 1.7 meter quartz prism spectrograph permitted the determination of the shock tube impurities and relative line intensities. Use of the latter instrument in conjunction with a tungsten ribbon calibration lamp and a step filter provided an absolute intensity standard. For the hydrogen plasma, relative and absolute spectral line intensities were obtained which permitted calculation of 10^{17} centimeters^{-3} and ~~4 ev for the number density and temperature respectively~~ peak temperatures of 4 ev.

The authors ~~wish to express their gratitude to Doctors~~ Richard M. Head and Earle B. Mayfield ~~of Aerospace Corporation for suggesting~~ the problem and their continual guidance in pursuing its solution, to Professor Raymond L. Kelly of the Naval Postgraduate School for his advice and assistance in spectroscopic procedures and analysis, and to numerous Aerospace Corporation personnel.

ion and electron densities to 10 to the 17th power/cucm

TABLE OF CONTENTS

LIST OF ILLUSTRATIONS

1. Introduction

In recent years, particular attention has been focused on spectroscopic diagnostics of plasma devices. Early investigations and preliminary theories were based on the results of flame, arc, and spark experiments. Refinement to these theories and formulation of new theories have emerged from sophistication of the earlier plasma devices to include among others that of the plasma shock tube. Within such a shock tube, the plasma is formed by transferring energy from a shock generator to the gas filling. The presence of the shock wave and subsequent energy transfer is evident from the appearance of a luminous shock wave within the tube, the properties of this wave being the subject of the spectroscopic studies.

The two spectroscopic instruments used in this shock tube investigation were the streak camera and the spectrograph. From these instruments, the derived experimental data permitted determination of the following plasma parameters:

a. shock tube impurities
b. luminous shock front velocity
c. electron and ionic temperatures
d. electron and ion number densities

Specific theories used to calculate these parameters include those of relative and absolute line intensities, line broadening, and apparent series limit. Throughout this paper, we have briefly mentioned each theory prior to applying the pertinent results derived. A more complete explanation of these theories will be found in the references provided.

The actual investigation was conducted at the Aerospace Corporation Physical Research Laboratory on two separate shock tubes, each briefly described in the next section. Calculations were initiated at Aerospace Corporation and completed at the U.S. Naval Postgraduate School.

It should be pointed out that not all of the previously mentioned plasma parameters were determined for each shock tube. Our study is only intended as a preliminary investigation to future additional and more extensive studies to be performed on both shock tubes.

2. Experimental Set-up

Components comprising the experimental set-up may be generally divided into shock tubes, magnetic piston driver and related power components, gas supply and vacuum system, and monitor and test equipment. A photograph, Fig. 1, shows the physical placement of the experimental set-up during a spectroscopic investigation. A schematic of the experimental setup is shown in Fig. 2. In this section, only a brief description will be given of the components mentioned above.

A. Shock tubes

The first shock tube placed under investigation was a General Electric, type 204, fused quartz tube. Approximate dimensions were 45 inches in length with inside and outside diameters of 74 and 79 mm, respectively. A chemical analysis by the manufacturer was conducted to determine tube material impurities (see Table I). Prior to making a spectroscopic investigation, the tube was modified by the placement of two replaceable one-inch diameter flat optical quality sapphire windows about 10 and 20 centimeters from the driver assembly. The latter modification prevented the necessity of making spectral observations through cloudy tube inner surface impurity film deposits.

The second shock tube was rectangular in shape and was fabricated of aluminum by Aerospace Corporation. Approximate dimensions were an overall length of 36 inches and an inner and outer dimension of three and four inches square respectively. Spectroscopic observations were made through six inch diameter optical quality fused quartz windows 12.6 inches from the driver assembly. The smaller windows as noted in Fig. 3 closer to the driver assembly were for later investigations (interferometric) to be conducted on the shock tube.

B. Magnetic Piston Driver and Related Power Components

The magnetic piston driver was a modified form of the "conical shock tube" type[1]. Power for the magnetic field driver was

derived from a 40 KV potential between a capacitor bank of eight General Electric (type 14F97) 1.0μf can capacitors (25 KV) and a floating ground strap at a negative 15 KV potential (see Fig. 2.).

C. Gas Supply and Vacuum System

The vacuum system consisted of a fore pump, diffusion pump, and liquid nitrogen trap, an arrangement providing pressures as low as 10^{-6} cm Hg. Vacuum gauges used were a Veeco, type RG-2A (pressures less than 100μHg) and a Autovac, type 3294B (pressures above 100μHg). In addition, a purge pump was incorporated into the gas supply line. The gas supply system consisted of bottled gas and associated tubing and valve components.

D. Monitor and Test Equipment

The major components of moniter and test equipment were:

1) Gaertner Scientific Corporation Quartz Spectrograph, type L 254
2) Philips Research Laboratories Tungsten Ribbon Lamp, type W2 (with intensity calibration)

Additional equipment used in data reduction included:

1) Leeds and Northrup Recording Microphotometer, type 6700-2
2) McPherson Instrument Measuring Comparator, type 100

3. Investigation Procedures

A brief discussion is made below outlining the preliminary tests made on the shock tube system. Mention is then made of the procedures followed in the subsequent spectroscopic investigation.

A. Preliminary

The ringing frequency of the discharge circuit was determined by placing a pickup coil about one-half inch above the return straps of the driver assembly. Analysis of an oscilloscope Polaroid picture of the coil signal revealed a discharge circuit ringing frequency of 245 KC.

The luminous shock wave produced in the fused quartz shock tube was examined with a rotating mirror streak camera. Fig. 4 is an enlargement of a typical luminous shock wave velocity smear picture. The appearance of weak shock waves after the primary bright shock may be attributed to the ringing of the discharge circuit after firing. The heavy dark lines in Fig. 4 are reference distance markers along the shock tube axis. The entrance slit of the streak camera was aligned along the central shock tube axis in order that the 35 mm film strip yielded a plot of light intensity distribution along the tube axis versus time.

The velocity of the luminous shock front was determined as a function of initial Hydrogen and Deuterium inlet pressure so that the optimum inlet pressure for maximum shock velocity could be obtained *. Fig. 5 and 6 are curves of initial inlet pressure versus shock velocity for Hydrogen and Deuterium gases respectively. The optimum pressures for maximum shock velocities were determined to be 80μ of Hydrogen and 125μ of Deuterium yielding maximum shock velocities of 17.22 cm/μ sec and 11.65 cm/μ sec respectively.

* The method used to calculate the velocity of the luminous shock front is shown in Appendix I.

B. Spectroscopic

Prior to firing either shock tube, the system was evacuated to about 10^{-5} cm Hg pressure. The gas supply line was then purged, after which the gas to be ionized, hydrogen or deuterium, was flushed through the system at approximately 100 microns pressure for periods in excess of 15 minutes. The gas pressure was then regulated to that pressure corresponding to maximum luminous shock front velocity and the tube fired. Between tube firings, flushing occurred during which time the system returned to the desired pressure without any readjustment of the gas supply system.

4. Relative and Absolute Line Intensities

Both relative and absolute line intensities are utilized in the spectroscopic calculation of electron temperature and number density. A tungsten ribbon standard lamp exposure on the same spectroscopic plate with the experimental exposures provides the reference for absolute and relative intensity calculations. Densitometer traces were made of the standard lamp and experimental exposures. Accepted data reduction procedures [2,3,4] were then used in the calculation of relative and absolute line intensities.

A. Relative Line Intensity

In the calculation of relative intensities, the spectroscopic plate was calibrated using the standard lamp source in order to account for the change in emulsion sensitivity with wavelength and the non-linear dispersion of the spectrograph used. A calibation curve was then plotted, Fig. 7, which relates observed line intensities at all wavelengths to a common intensity scale as follows:

$$\left(\frac{I_1}{I_2}\right)_{\text{corrected}} = \frac{B(\lambda_1)}{B(\lambda_2)} \left(\frac{I_1}{I_a}\right)_{\text{observed}} \qquad (4\text{-}1)$$

where $B(\lambda)$ is the correction factor which depends on emulsion sensitivity and spectrograph dispersion.

The corrected relative line intensities were:

Element	Multiplet[5,6]	Wavelength	Relative Intensity normalized to H_α
H_α		6563	1.00
H_β		4861	0.0282
H_γ		4340	0.00905
H_δ		4102	0.00370
H_ε		3970	0.00155
O II	3	3749	0.0211
O II	36	4190	0.00346
O II	2	4349	0.0106
O II	5	4415	0.00780
O II	1	4649	0.0150
Ca II	4	3179	0.0455
Ca II	3	3737	0.00308
Ca II	1	3934	0.0843
Ca II	1	3968	0.0575
Mg II	1	2796	1.02
Mg II	1	2803	0.906
Mg II	3	2798	0.262
Mg II	2	2936	0.124
Ti II	2	3235	0.105
Ti II	2	3242	0.0555
Ti II	1	3349	0.118
Na I	6	5688	0.00628
Na I	1	5890	0.360
Na I	1	5896	0.310
Na I	5	6161	0.0141
C II	6	3921	0.00410
C II	4	4267	0.0374

B. Absolute Line Intensities

The absolute line intensities for the Balmer series lines were calculated separately for H_α through H_ϵ using calibrated standard lamp exposures for each of these wavelengths in the general method described by Harrison, Lord, and Loofbourow[4].

Several assumptions were made:

1) In order to obtain a value for the spectroscopic system transmission factor, the following representative transmission values were assumed[4]:
   a. 0.90 for each lens
   b. 0.85 for each prism
   c. 1.00 for each mirror

In order to minimize the error involved in this assumption, the standard source was used with the same optical parameters that were used in the experiment[7].

2) The path length from the standard lamp to the entrance slit was sufficiently short to avoid appreciable horizontal extinction of the standard source radiant energy[7].
3) To obtain the radiant energy, the solid angle subtended by the collimator at the slit was approximated by[4]:

$$W = \frac{A}{F^2} \qquad (4\text{-}2)$$

where W = solid angle subtended by the collimator at the slit

A = area of the collimator

F = collimator focal length

4) The vertical variation of the emulsion was negligible.
5) The time of radiation was approximately 5×10^{-6} seconds. This time corresponds to the duration of the bright region in the smear photograph, Fig. 3.
6) The shock tube was optically thin[8].

The absolute energies and intensities calculated per shock tube firing were:

Line	Energy (ergs)	Intensity ($ergs\text{-}cm^{-2}\text{-}sec^{-1}\text{-}ster^{-1}$)
H_α	1.353×10^{-4}	0.6950×10^{7}
H_β	0.386	0.1980
H_γ	0.133	0.0683
H_δ	0.0288	0.01478
H_ϵ	0.0220	0.01130

5. Shock Tube Impurities

The identification of shock tube impurities for both shock tubes, although a tedious procedure, was of primary interest and produced a useful result. Following the extension of the spectrograph calibration curve to include the 2000-7000 Å range, shock tube firings were conducted under the conditions shown in Table II. In conjunction with the above mentioned curve and comparator measurements, line wavelengths were obtained. A typical 3400 Å center wavelength spectrum is shown in Fig. 8. Element and multiplet identification was then made using tables prepared by Charlotte Moore[5,6]. Line identification results are shown in Table III and are valid for both the fused quartz shock tube and fused-quartz-window aluminum shock tube. This impurity spectra corresponds to the known constituents of the shock tube electrodes and walls and verifies that ablation occurs during shock tube firing. This result will prove useful in impurity identification in similar shock tube systems employing fused quartz surfaces as spectral windows.

6. Electron Number Densities

A knowledge of number densities is necessary in several of the methods for determining electron temperature. Two approaches to number density calculation are those of A. apparent series limit and B. the Stark broadening profile comparison. The formulation of a hydrogen plasma clearly validates the assumption of equating electron and ionic number densities.

A. Apparent Series Limit

As the principal quantum number, m, of a Balmer line increases, Stark broadening of that line increases. Therefore, these lines merge and form an apparent continum. Inglis and Teller[9] derived a relationship between the last discernible line before the resulting apparent continum and number density for application to astrophysical observations. A slight modification to their equation was made by Lochte-Holtgreven[8] for use with radiating plasma observations. This relationship is:

$$\text{Log } N = 23.46 - 7.5 \text{ Log } m_{max} \qquad (6\text{-}1)$$

where $N = n_e = n_i$ = number density

m_{max} = principal quantum number of the last discernible line within the series.

Letting $m_{max} = 7$ for H_ϵ (see Table III) results in the values:

$$n_e = n_i = 1.3 \times 10^{17} \text{ cm}^{-3}.$$

B. Stark Broadening Profile

For particularly broad Balmer line profiles, it may be assumed linear Stark broadening is dominant. Among the initial treatments of this phenomenon was that of Holtzmark, who considered only the effects of perturbing ions on the emitting atoms[8]. As this theory did not closely agree with experimental line profile observations, further refinement of this theory was formulated by Griem, Kolb, and Shen[10] and included the perturbing effects of both electrons and ions on the hydrogen atoms. The experimental line profiles of H_α and H_β are shown

in Fig. 9 and 10, each a plot of normalized line intensity, I/I_o, versus displacement from center wavelength, $\Delta\lambda$. Theoretical profiles, as determined by Griem, Kolb, and Shen[10] are also shown superimposed on the experimental profiles. In plotting the theoretical profiles, the useful relationships developed were[10]:

$$\Delta\lambda = 1.25 \times 10^{9} N^{2/3} \alpha \qquad (6\text{-}2)$$

$$I/I_o = \frac{(\text{area})\, S(\alpha)}{0.625 \times 10^{-9} N^{2/3}} \qquad (6\text{-}3)$$

where N = electron number density.

α = ratio of the distance from the unperturbed line, $\Delta\lambda$, to the Holtzmark normal field strength, $F_o = 2.61\, eN^{2/3}$

$S(\alpha)$ = line profile function such that $\int_{-\infty}^{\infty} S(\alpha)\, d\alpha = 1$.

(area) = area under the normalized experimental line profile.

Reference to Fig. 9 and 10 indicates that the effect of temperature is small and that of number density is predominant in determining the theoretical profile. From the curve fitting then, it can be seen that

$$10^{16} < N < 10^{17}$$

where $N = n_e = n_i$ in centimeters^{-3}

In the calculations of electron temperature to follow, it will be assumed that electron and ionic number densities equal 10^{17} centimeters^{-3}. This approximation is borne out by the above calculations and is considered accurate within an order of magnitude.

7. Electron Temperature Determination

The temperature of a plasma may be defined only if there is statistical or thermal equilibrium[11,12]. Assuming thermal equilibrium, the population distribution over the excited energy levels varies according to Boltzmann's law. The spectral intensity may therefore be related to the temperature.

The intensity of an emission line corresponding to a transition from n to m is given by:

$$I_{nm} = B\,W^{nm}\,h\nu_{nm} = BA^{nm}\,N_n\,h\nu_{nm} \qquad (7\text{-}1)$$

where B = instrumental constant

$W^{nm} = N_n\,A^{nm} = \dfrac{\text{number of transitions taking place in light source}}{\text{second}}$

N_n = number of atoms in initial state n

A^{nm} = Einstein transition probability = $\dfrac{\text{number of transitions of atom}}{\text{second}}$

$h\nu_{nm}$ = radiated photon energy

For the case of thermal or statistical equilibrium, the population distribution may be defined as:

$$N_n = \frac{Ng_n}{u}\ \exp\left(-E_n/k\,T_e\right) \qquad (7\text{-}2)$$

where N = total density of emitting species in volume for which the intensity is being measured.

g_n = degeneracy of initial state n (statistical weight)

u = partition function of all statistical weights

E_n = energy of the initial state n above ground state

T_e = election temperature

Also[13], $g_n\,A^{nm} = 2/3 \times 10^{16}\,g_j f_j/\lambda^2 \qquad (7\text{-}3)$

where j = 1 or 2

λ = wavelength of the transition

f_1 = oscillator strength determined for absorption

f_2 = oscillator strength determined for emission

$g_n = g_2$ = statistical weight of the initial state n

g_1 = statistical weight of the final state m

Therefore,

$$I_{nm} = D\nu_{nm}^3 (g_n f_n) \exp(-E_n/k T_e) \qquad (7\text{-}4)$$

where $D = \left(\frac{BNh}{u}\right) (2/3 \times 10^{16}) \left(\frac{1}{c^2}\right)$

Equation 7-4 may be used with the absolute intensity of a single line in order to determine the electron temperature, but this method is difficult due to the uncertainty in the total density, N, of the plasma. In calculating N, it is necessary to determine the density of each constituent present, requiring additional assumptions to those already made[8]. Also, there is uncertainty of reproducing the same constituent densities with each tube firing due to the variable effects of ablation in the shock tube.

Several methods were attempted in the determination of electron temperature.

Method I: Relative Intensity

Equation 7-4 may be rearranged as follows:

$$\text{Log}\left(\frac{I_{nm}}{D\nu_{nm}^3 g_n f_n}\right) = -\frac{E_n \log e}{kT_e} \qquad (7\text{-}5)$$

Since D is independent of the energy E_n, it may take any value and the left hand side of 7-5 may be expressed in arbitrary units[13]. In the calculation of temperature using the lines from an element, the relative intensities and relative values of $(g_n f_n)$ may be used[13,14]. A plot of

$$\log\left(\frac{I_{nm}}{\nu_{nm}^3 g_n f_n}\right)$$

versus E_n for a number of lines from an element should therefore result in a straight line with slope $= -\frac{1}{kT_e}$ Log e.

Method II: Relative Intensity Ratios

Equation 7-4 may also be formed into a ratio of two lines from the same element, giving the resultant equation:

$$\text{Log}\left(\frac{I_1\nu_2^3 g_2 f_2}{I_2\nu_1^3 g_1 f_1}\right) = -\left(\frac{E_1 - E_2}{kT_e}\right)\text{Log } e \qquad (7\text{-}6)$$

Since ratios are being used any arbitrary consistent units may be used for I, ν and (gf). A plot of

$$\log\left(\frac{I_1\nu_2^3 g_2 f_2}{I_2\nu_1^3 g_1 f_1}\right)$$

versus $(E_1 - E_2)$ for a number of pairs of lines from an element should therefore result in a straight line with slope $= -\frac{1}{kT_e}\log e$.

In Methods I and II, the resultant graphs, a sample shown in Fig. 11, not only yield a value for the electron temperature, but also act as a quasi-check for the assumptions of thermal equilibrium. If the resultant points do not fall on a straight line and the data has been checked for systematic errors, then any curvature indicates a lack of thermal equilibrium in the population of the excited states of the constituents and no temperature can be defined (this curving was not observed in our results).[11,13]

Method III Absolute Intensity

The absolute intensity of the Balmer lines in emission may be used in the electron temperature determination as follows:[15]

$$I_{abs} = \frac{\pi e^2 h f n^2 N_o \ell}{m_e \lambda^3}\exp\left(\frac{-E_n + E_o}{kT_e}\right) \qquad (7\text{-}7)$$

where e = electron charge

h = Planck's constant

f = oscillator strength

n = principle quantum number of the upper state

N_o = neutral atom number density

l = radiating layer thickness

m_e = electron mass

λ = emission line wave length

E_n = energy of the state n

E_o = energy of the ground state = - 13.595 ev

The depression of ionization potential within the plasma is a result of the presence of ions which are a finite distance apart. The effect of the ions is to alter the Coulombic field in which the electrons move and may be expressed as:[8]

$$\Delta E = 7.0 \times 10^{-7} N_e^{1/3} \text{ ev} \tag{7-8}$$

where N_e = electron number density.

This corresponds to a depression of 0.32 ev with $N_e = 10^{17}$ cm^{-3}.

Assuming that the thickness of the radiating layer is approximately given by the shock tube diameter[16] and substituting the electron number density determined earlier, equations 7-7 and 7-8 reduce to:

$$T_e = \frac{-1.16 \times 10^4 (13.28 + E_n)}{36.77 + \ell n \left(\frac{I_{abs} \lambda^3}{n^2 f N_o} \right)} \tag{7-9}$$

where T is in degrees Kelvin, N_o in $(\text{centimeters})^{-3}$, λ in centimeters, I_{abs} in ergs-cm^{-2} -sec^{-1} -$ster^{-1}$., E_n in electron-volts, and f and n are dimensionless.

Equation 7-9 may be solved for any of the Balmer lines in emission if the neutral atom number density can be obtained. This latter quantity was assumed equal to the electron number density, that is 50 percent ionization. The effect of this assumption is discussed in the next section.

Results of the electron temperature calculations are:

Method	Element	Temperature degree Kelvin	e-v
I	H	6,300	0.54
I	Na I	50,000	4.30
I	Ca II	10,800	0.93
I	C II	31,300	2.70
I	Mg II	24,800	2.14
I	Ti II	6,600	0.57
II	H	6,800	0.59
II	Na I	47,000	4.05
II	O II	24,000	2.07
III	H_α	7,910	0.68
III	H_β	7,890	0.68
III	H_γ	7,730	0.67
III	H_δ	7,300	0.63
III	H_ε	7,300	0.63

8. Discussion

The calculation of accurate temperatures, power levels, and densities in a plasma is very important. Aside from the ability to describe accurately the physical parameters of the plasma system, these values enable the further derivation of experimental transition probabilities and the calculation of collision cross-sections which to date are not sufficiently known.

In association with Doctor Richard M. Head, considerable time was devoted to identification of the various impurities present in the shock tubes[17]. Since the observed impurity spectrum was identical for the quartz shock tube and for the aluminum shock tube with quartz windows, it is felt that the list of spectral lines shown in Table III will be of assistance in impurity identification for most quartz systems operating under similar conditions. It should be pointed out that only those elements that could contribute significantly to the intensity of a particular line are included in Table III. There were, in addition to the listed wavelengths, some 100 lines that were of very low intensity which are omitted due to uncertainty in their origin. Also, most of the lines below 2800 Å are omitted because of limited identification data in this region.

Using the spectral lines of the various impurities in the calculation of temperature, a check may be made on whether a unique temperature can be defined for the plasma[16].

The accuracy of the calculated temperature and number densities in the shock tube is highly dependent on the relative and absolute line intensities obtained. In order to determine correctly the relative or absolute intensity of a line, a number of factors must be carefully considered. These include:

1) Spectroscopic techniques used
2) background continum correction
3) plate-calibration corrections for
   a) dispersion
   b) emulsion sensitivity
   c) standard source
4) self-absorption considerations
5) computational errors

The first three correction factors were determined using standard spectroscopic techniques described in Harrison, Lord, and Loofbourow[4], and with the special techniques mentioned in appendix II.

The problem of self-absorption, if present, can seriously affect the measured intensities of the lines, and therefore lead to meaningless results. Severe self-absorption is characterized by flat-topped lines or separation of one line into two lines by strong absorption in the middle of the spectral line[13]. For plasma systems operating at temperatures greater than approximately one ev, the problem of self-absorption is lessened.[8] Such absorption is related to the total intensity of emission from an element, which is temperature (energy) dependent, and the total number of potential absorbers. At temperatures (energies) near the maximum intensity of emission, the amount of absorption becomes negligible since the number of absorbers present is much less than the number required to absorb all of the emitted energy. For hydrogen, this temperature corresponds to approximately one ev. As severe self-absorption was not observed, the system was therefore assumed to be optically thin for the Balmer series. Future experimental work with this system should include a check on the validity of the optically thin plasma assumption by placing a mirror on the optical axis behind the source, as recommended by Pearce[13].

Since neither radial distribution not time resolution studies were conducted in this experiment, the intensities determined permit only the calculation of a mean integrated temperature for the plasma[14].

Taking into account the above considerations, it is believed that the intensities calculated are representative of the populations of the various energy states and consequently may be used in temperature and number density calculations using the Boltzmann distribution.

The two methods, apparent series limit and Stark Broadening profile comparison, employed to determine number densities are based on the existance of line broadening phenomena. They are, however, unrelated as to the parameters being considered.

In the method of the apparent series limit, there is no known limitation placed on equation 6-1 other than a decrease in the calculated value

by a factor of two in number density if the plasma temperature is less than $10^5 / m_{max}$ (where $m_{max} = 7$ in our study)[8]. This seems unlikely from the temperature calculations in this research.

In the method of Stark broadening profile comparison, the range of applicability for experimental profiles provided is $10^{14} \leq n_e \text{ cm}^{-3} \leq 10^{19}$ and $10{,}000 \leq T\ ^{\circ}K \leq 40{,}000$. As previously mentioned, the effect of number density variation is dominant over that of temperature variation. The accuracy of the theoretical profiles is approximately ten percent[10], and the accuracy of experimental profiles used are estimated to be of this same order of magnitude. The experimental accuracy is not quite as high for succeeding lines in the Balmer series because of masking of the wings by impurities. The choice of 10^{17} cm^{-3} must be within an order of magnitude for electron number density since it appears consistent with the results of 1.3×10^{17} cm^{-3} and $10^{16} < n_e \text{ cm}^{-3} < 10^{17}$ by the series limit and Stark broadening methods respectively.

Prior to electron temperature calculation using absolute intensities, it was necessary to estimate the neutral atom number density. The value 10^{17} cm^{-3} was decided upon with the stipulation of studying its variation as a parameter. Variation of neutral atom number density by two orders of magnitude affected the resulting electron temperature by less than a factor of two. In view of this result, it is not belived that the electron temperature results are materially affected by the necessity of this procedure.

In the determination of electron temperature, the calculations were limited by the lack of transition probabilities for many of the observed lines[18]. In methods I and II the accuracy of the results depends strongly on the properties of the lines used in the calculations. It is very desirable to choose a number of lines originating from a wide range of upper energy levels and occurring over a small wavelength interval[14]. This procedure was somewhat compromised due to the lack of transition probabilities. The range of validity of methods I and II is up to approximately $5 \times 10^5\ ^{\circ}K$ with the proper selection of the elements[8]. For each wavelength line there is a relatively flat maximum in the temperature-intensity profile which extends over a few thousand degrees. Therefore, when measuring a temperature,

it is more accurate to select a line where the slope of the temperature-intensity profile is rapidly changing. From data presented by Lochte-Holtgreven[8], the temperatures determined using Oxygen II and the Balmer lines were on the rapidly rising slopes of the temperature-intensity profiles and thus in the more accurate range. Similar data were not available for the other elements.

Since the electron density is relatively high (10^{17} cm^{-3}), there is a rapid approach to local thermodynamic equilibrium. The formula for relaxation time is given by Spitzer[19]:

$$t \simeq \frac{11.4\ A^{1/2}}{N\ Z^4\ \ln\Lambda}\ (T^{3/2})\ \text{sec.}$$

where $\ln\Lambda \simeq 20$

$A = 1$ for a hydrogen plasma

$Z = 1$ for a hydrogen plasma .

$N = 10^{17}\ cm^{-3}$

$T = 6270^{\circ}$ K (0.54 ev)

Therefore $t \simeq 10^{-10}$ seconds or less, and the concept of electron temperature has some meaning in the usual statistical sense. This is further verified by the results of calculations used in methods I and II. In these methods a marked departure from equilibrium is characterized by a curving, or trend, in the graphic data[13]. This curving, and hence departure from equilibrium, was not observed in our result (see Fig. 11). Several other advantages were gained by using methods I and II. A greater number of lines could be used with these methods than in the absolute intensity method; and therefore, any anomally caused by an improper f-value, self-absorption, or intensity error (which would result in a wide variation from the other values) could be easily distinguished. In addition the more easily measured relative intensity may be used instead of absolute intensity, and it is not necessary to know accurately the composition of the plasma.

The temperatures calculated by methods I through III varied from 0.54 to 4.2 ev. This result is to be expected, since each plasma constituent is likely to exhibit a different temperature during the time integrated observation. Future investigations should include a temperature-time variation study within the shock tubes.

The results of method III using the absolute intensity agree closely with the electron temperature calculated using the relative intensities of the Balmer lines. The difference between the methods, which is less than a factor of 25 percent, shows that the assumptions made in method III and those used in the absolute intensity calculations were reasonable.

The ion temperature may be estimated using the results of the absolute intensity measurements. This problem has been investigated theoretically for a pure hydrogen plasma considering the following factors[20]:

1) Energy transfer from atoms to electrons caused by elastic collisions between atoms and electrons and ions and electrons.
2) The energy dissipation by the electrons that is determined by:
   a) inelastic collisions of electrons with atoms and electrons.
   b) the excess of emission over absorption in free-free transitions.
   c) the excess of emission over absorption in free-bound and bound-free transitions.

The difference between electron and kinetic temperatures under these conditions would be:

$$T_i - T_e < 10^{-3} T_e$$

when $N_e > 10^{10}$ cm^{-3}

and $5000^{\circ}K < T_e < 10^{5}{}^{\circ}K$

From this relation the ion temperature is approximately equal to the electron temperature for the conditions existing in the shock tube (i.e., $N_e = 10^{17}$ cm^{-3} and $T_e \geq 0.54$ ev.).

9. Conclusions

A. Shock Tube Characteristics

Spectroscopic diagnostic techniques reveal the following plasma parameters existing within the two shock tubes with hydrogen introduced:

1) An electron and ionic number density of approximately 10^{17} cm^{-3},
2) A peak temperature of approximately 4 ev.
3) A condition of local thermodynamic equilibrium.

B. General

1) Shock tube systems employing quartz windows and operating under similar conditions are characterized by nearly identical impurity spectra.
2) Spectral line absolute intensity measurements provide a useful mechanism for determining plasma temperature.
3) Further investigation of the shock tubes under consideration should include time resolved and radial temperature and number density studies.

Fig. 1. Experimental Set-up During Spectroscopic Investigation

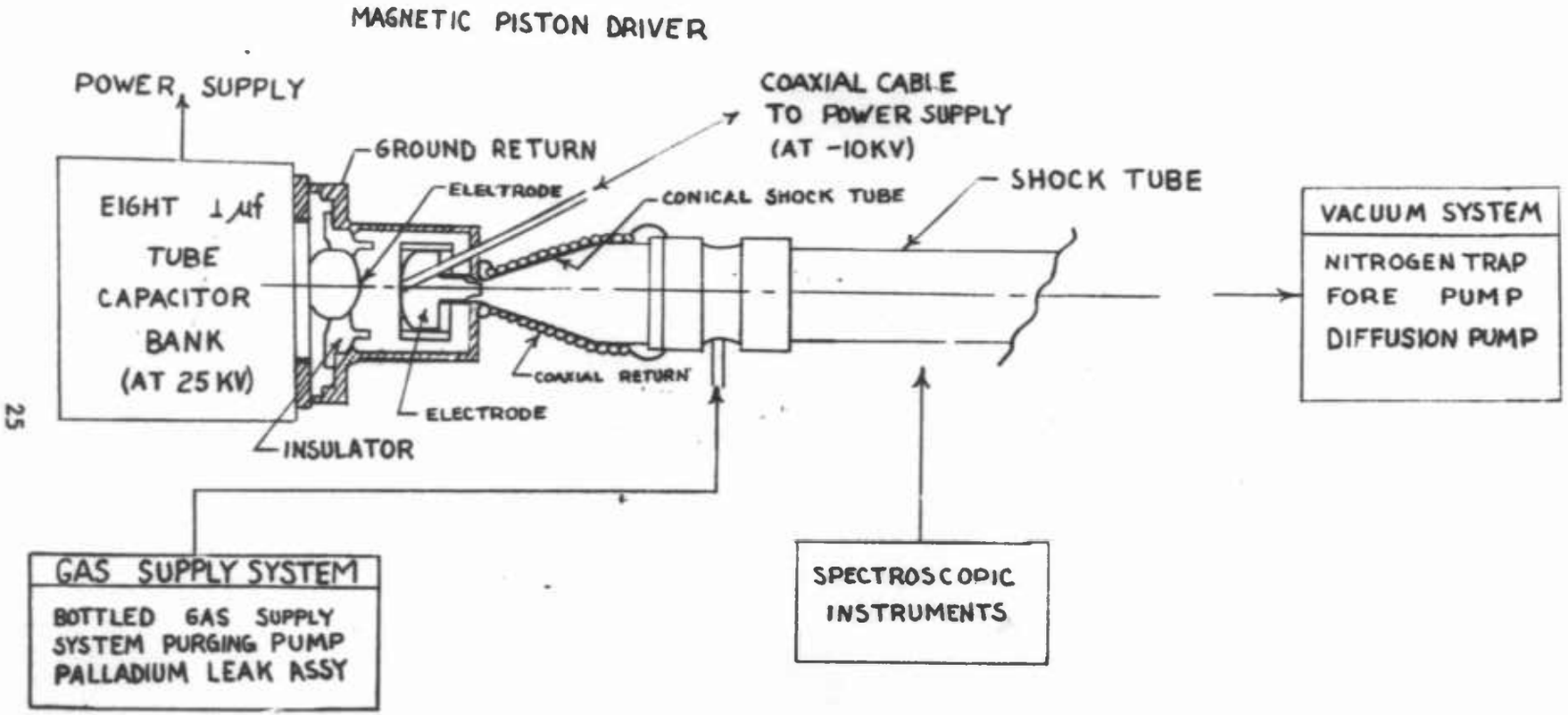

Fig. 2. Schematic of the Experimental Set-up

Fig. 3. Square Shock Tube

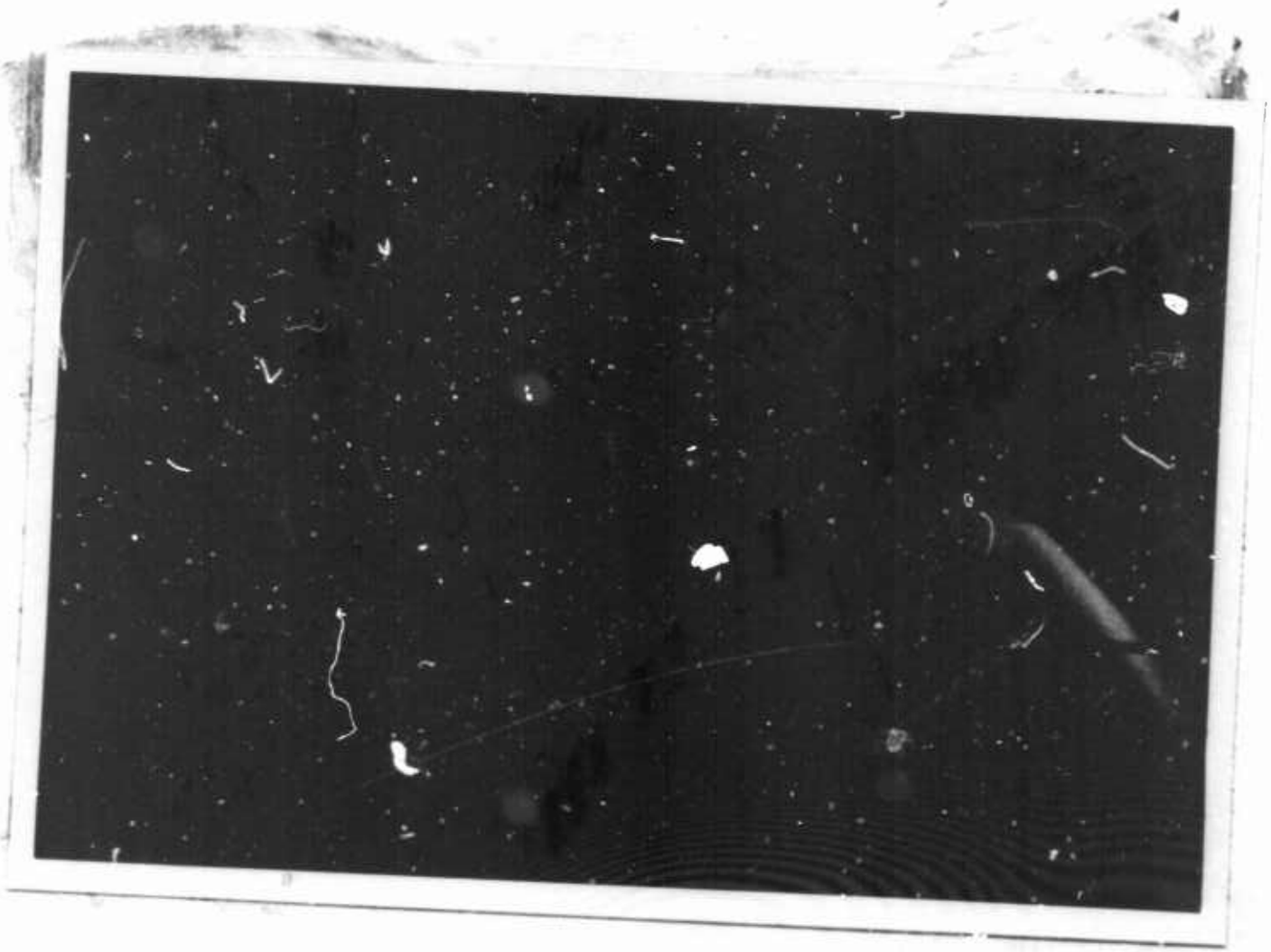

Fig. 4. Shock Wave Smear Photograph

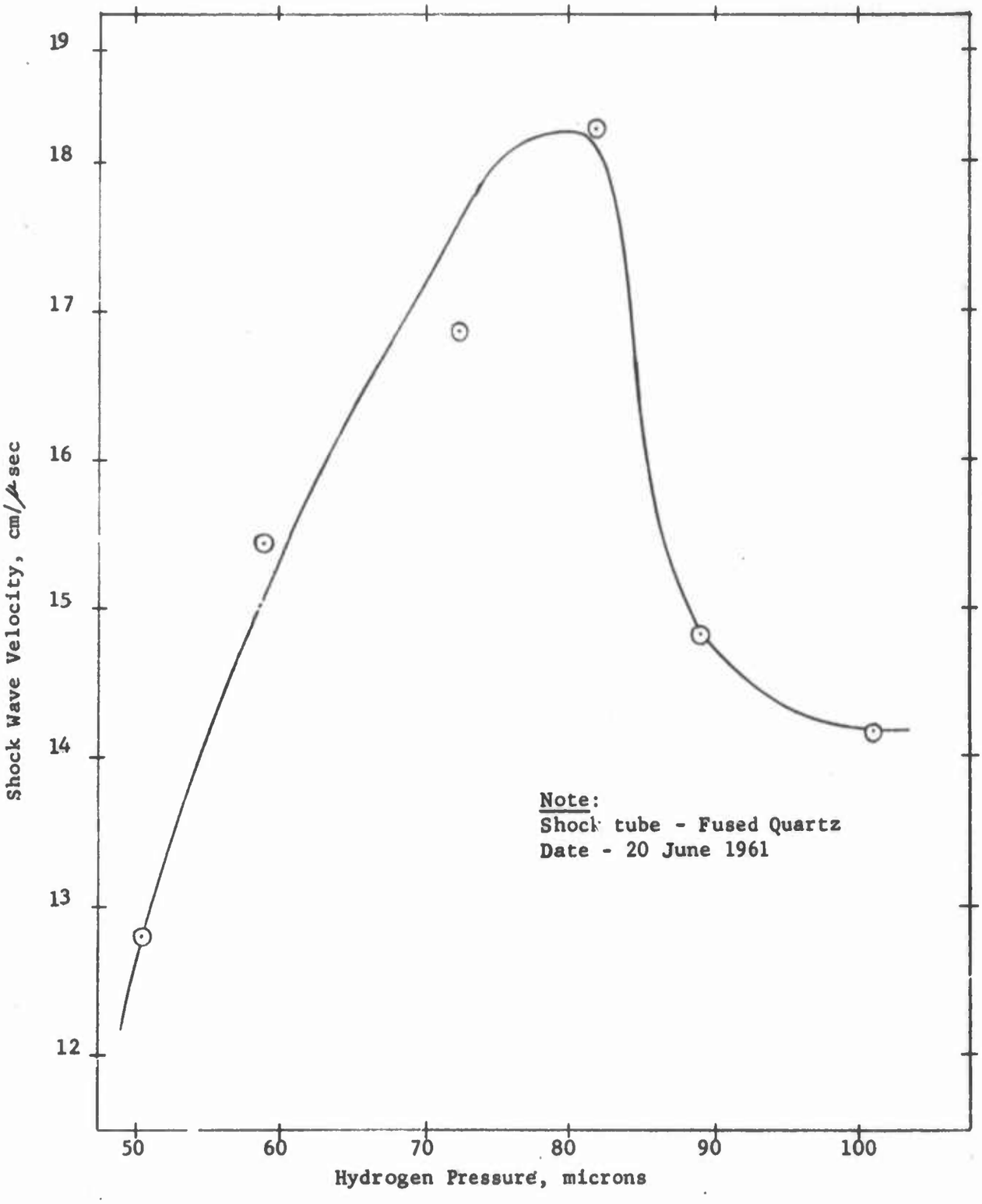

Fig. 5. Hydrogen Pressure Variation Effect on Shock Wave Velocity

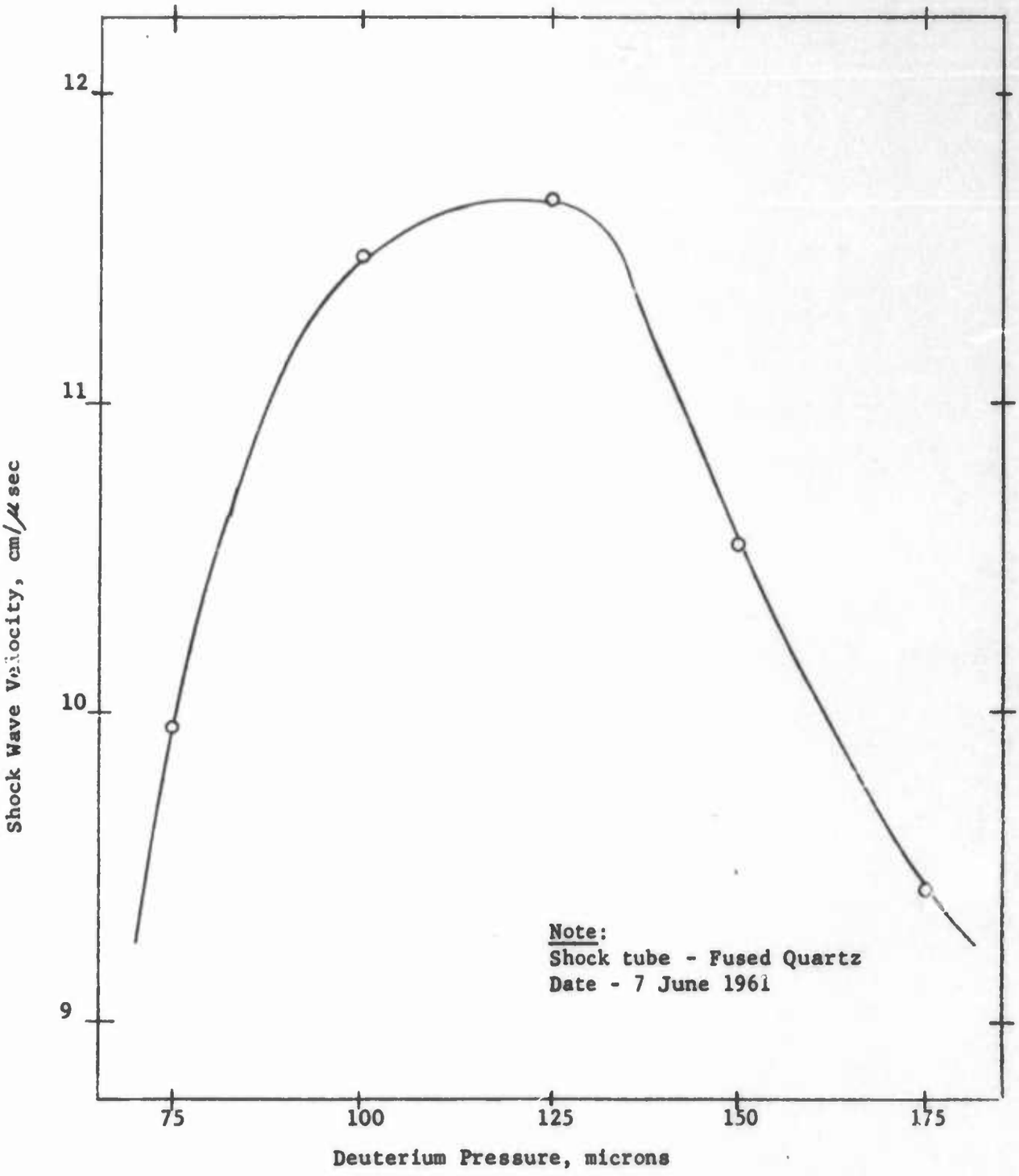

F g. 6. Deuterium Pressure Variation Effect on Shock Wave Velocity

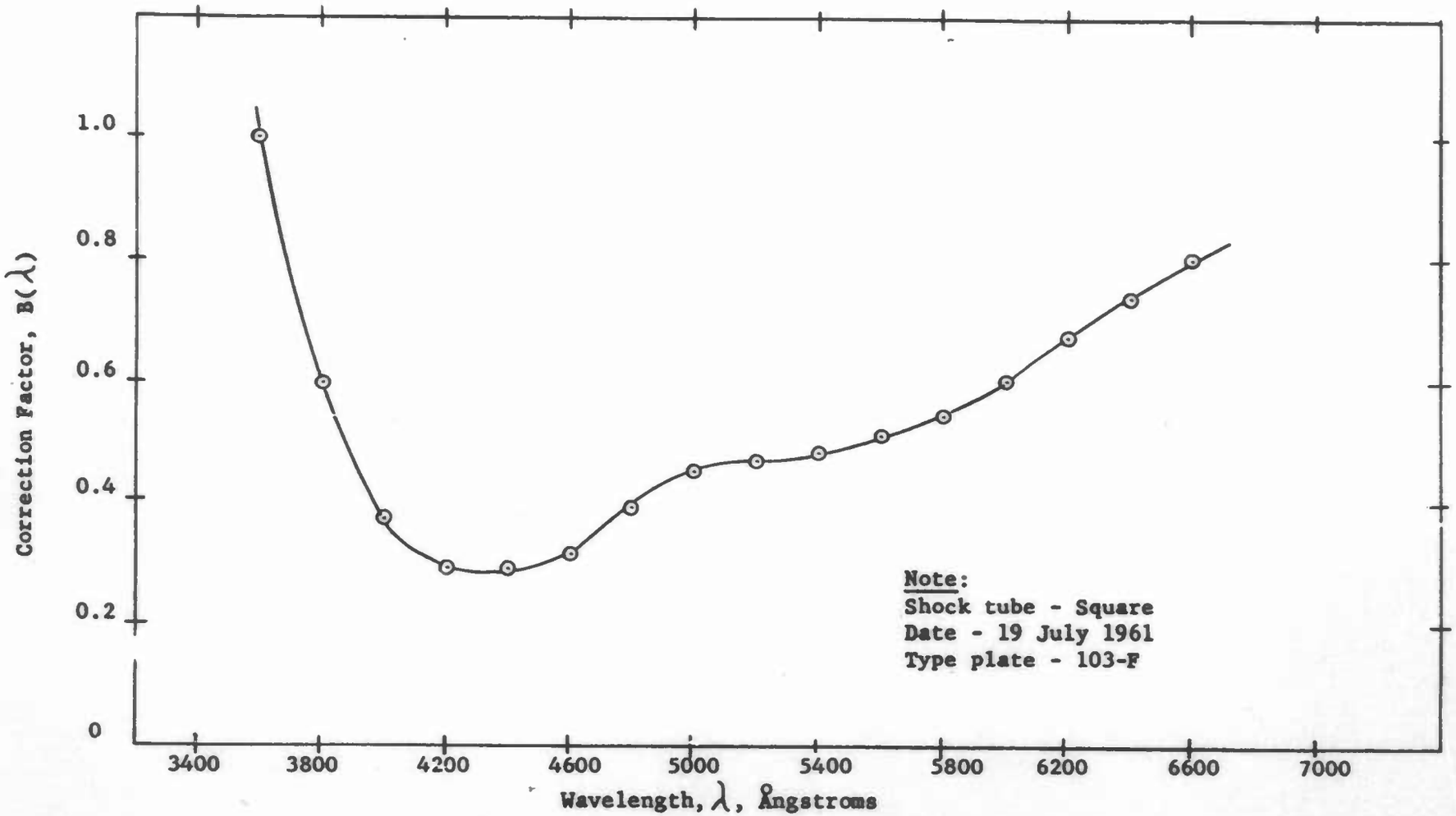

Fig. 7. Spectroscopic Plate Calibration Curve

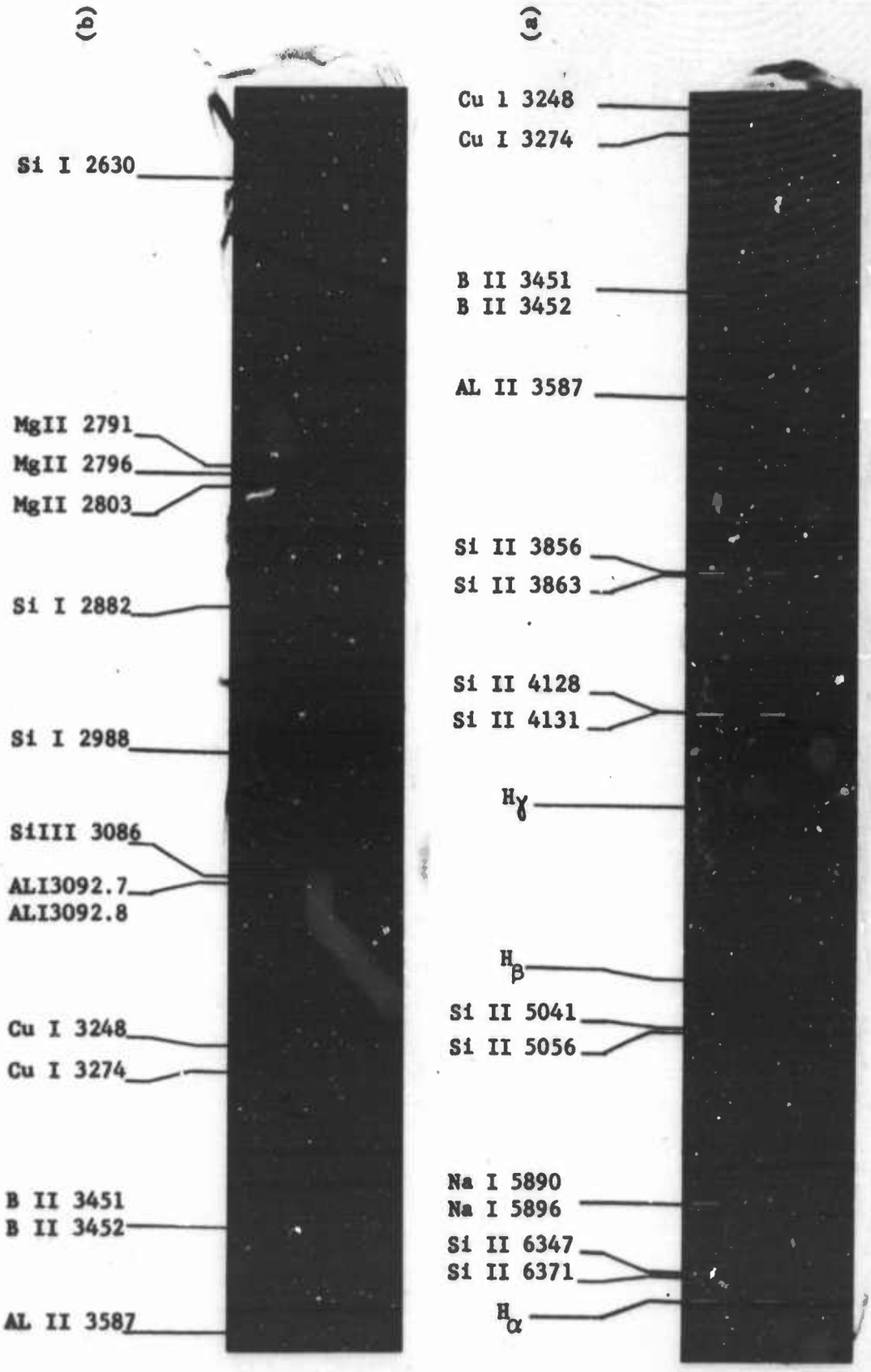

Note: a-plate 1 of 7/18, b-plate 1 of 7/10; see Table II for firing conditions; exposures from left to right - single shot, two shots superimposed, four shots superimposed.

Fig. 8. Typical Shock Tube Spectra

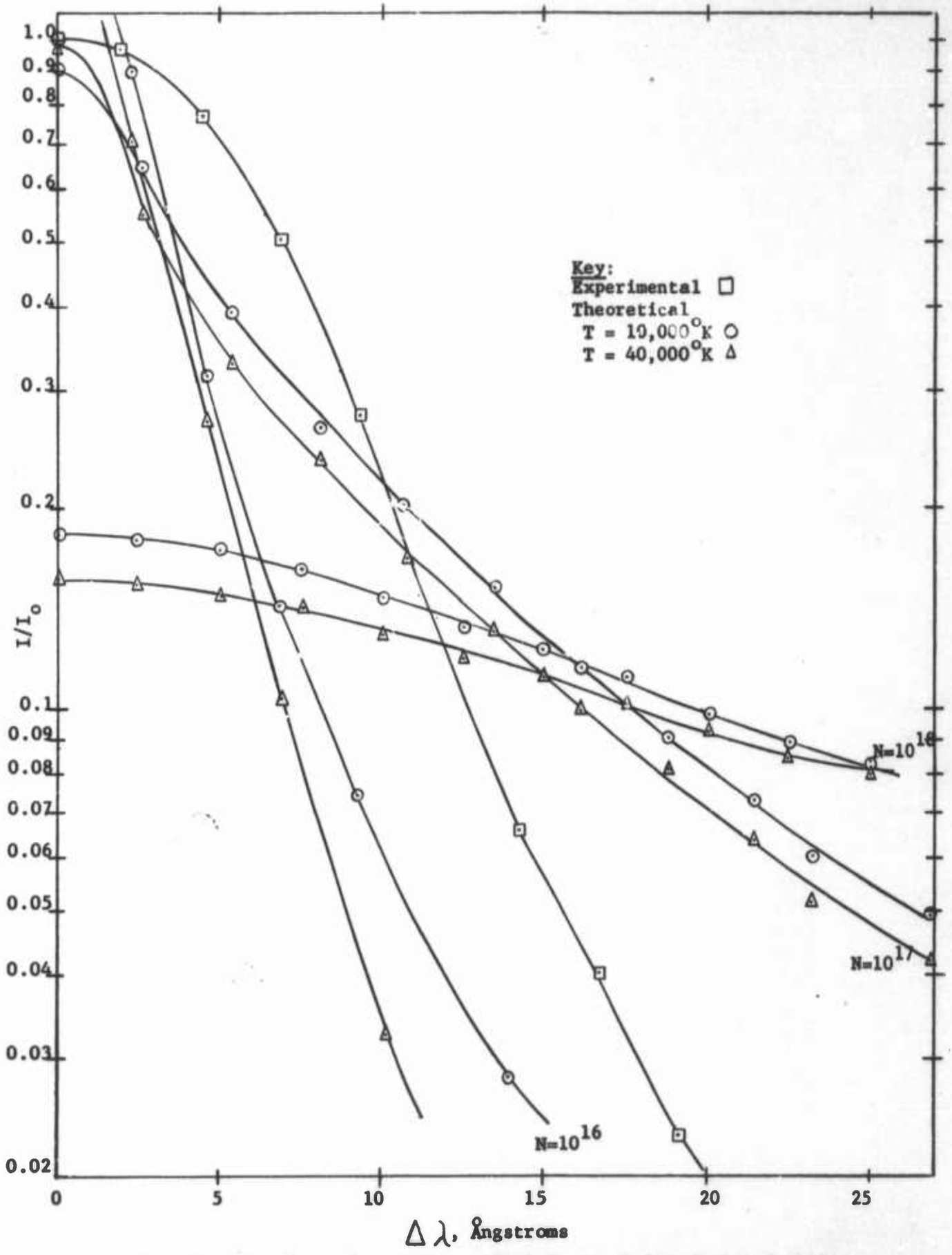

Fig. 9. Experimental and Theoretical H_α Stark Broadening Profiles

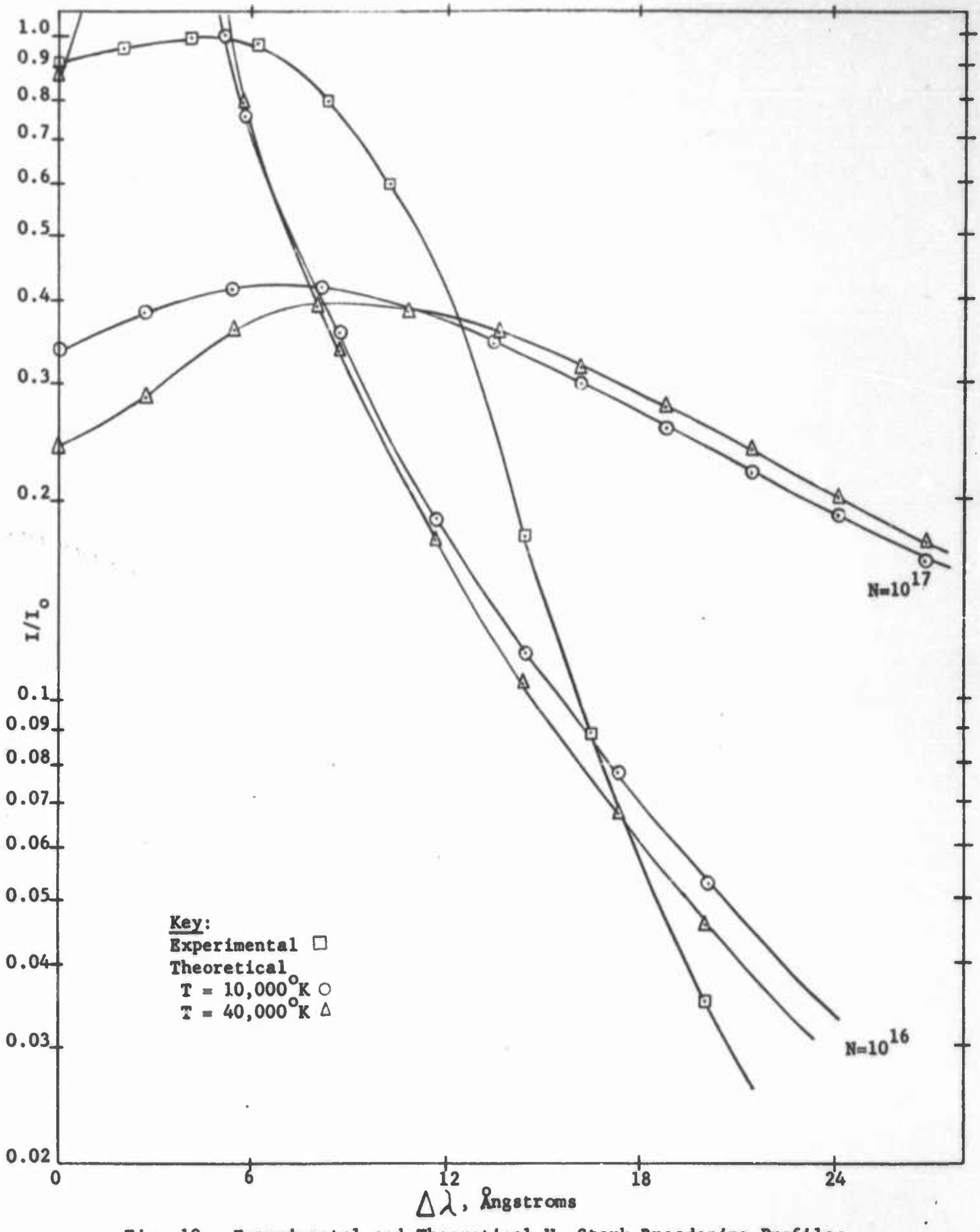

Fig. 10. Experimental and Theoretical H_β Stark Broadening Profiles

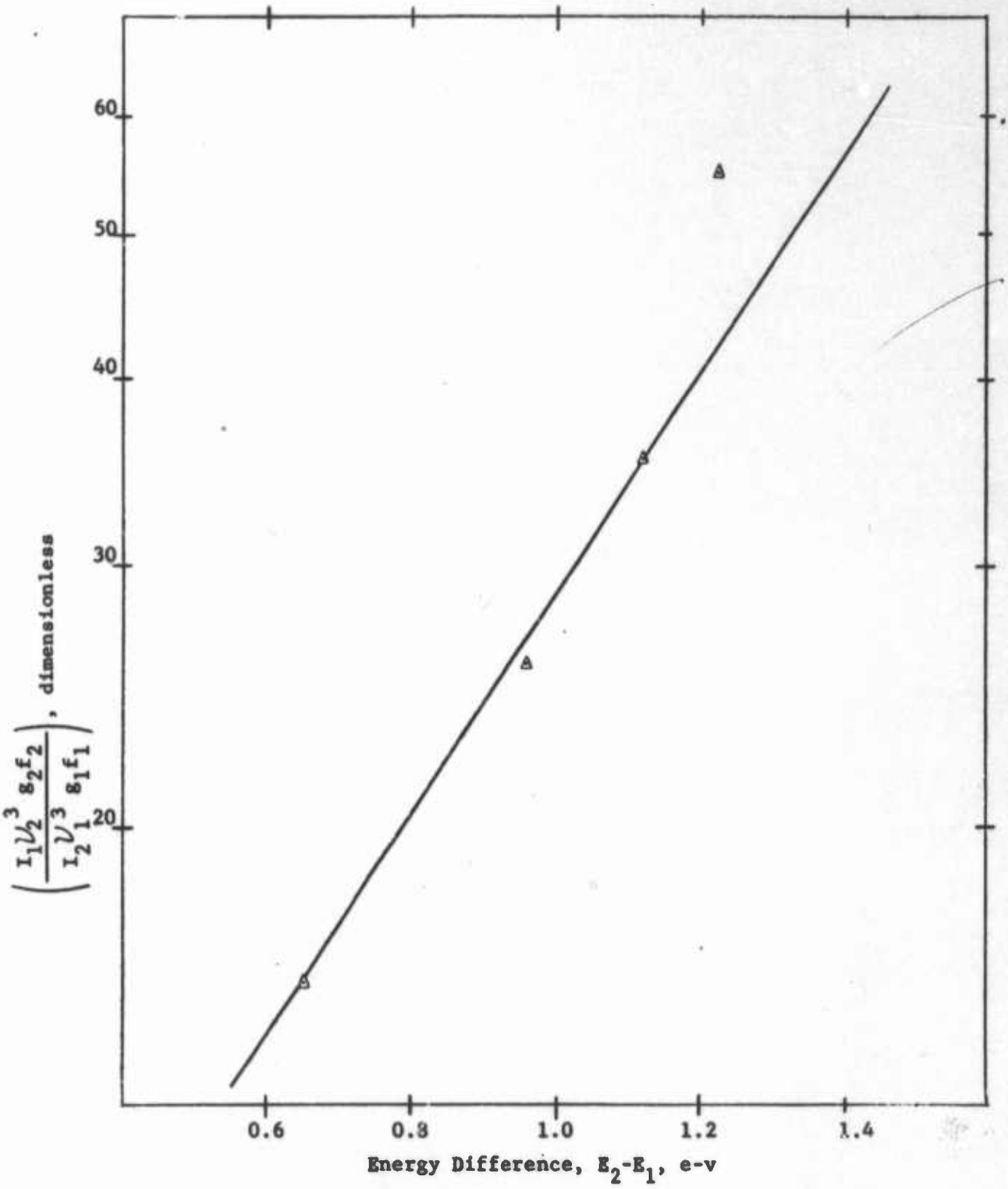

Fig. 11. Electron Temperature by Relative Intensities of Balmer Series

Impurity	Parts per Million
$Fe_2 O_3$	12
$Ti O_2$	4
$Al_2 O_3$	160
Ca O	22
$K_2 O$	6
$Na_2 O$	16
$Li_2 O$	9
B	0.94

Table I - Fused Quartz Tube Impurities as Provided by Manufacturer

Date	Shock Tube	Gas Filling	Gas Pressure, μHg	Film type	Center Wavelength, Å	Capacitor Charge, KV	Trigger Charge, KV	Remarks
6/9	Fused Quartz	D_2	125	35mm	----	25	-10	Streak Camera
6/20	Fused Quartz	H_2	varied	35mm	----	25	-10	Streak Camera
6/21	Fused Quartz	H_2	80	103-0	3400	25	-10	Spectrograph
6/23	Fused Quartz	H_2	80	SA-II	3400	25	-10	Spectrograph
6/26	Fused Quartz	H_2	80	1N	4300	25	-10	Spectrograph
7/6	Square	H_2	varied	35mm	----	25	-10	Streak Camera
7/10	Square	H_2	100	103-0	3400	25	-10	Spectrograph
7/11	Square	H_2	100	1N	4300	25	-10	Spectrograph
7/19	Square	H_2	100	103-F	3400	25	-10	Spectrograph at tube shots and std. lamp
7/19	Square	H_2	100	103a-0	3400	25	-10	

Table II - Typical Shock Tube Conditions during Spectroscopic Investigation

Table III Spectral Line Identification

Wavelength (Å)	Element	Multiplet[5,6] Number	Excitation Potential Low	Excitation Potential High	Relative Intensity (visual)
2367.064	Al I	4	0.01	5.21	10
2395.06	B II	4	12.64	17.79	6
2435.160	Si I	45	0.78	5.85	15
2478.556	C I	61	2.67	7.65	10
2496.773	B I	1	0.00	4.94	18
2497.724	B I	1	0.00	4.94	20
2506.896	Si I	1	0.01	4.93	18
2514.315	Si I	1	0.00	4.91	16
2516.109	Si I	1	0.03	4.93	20
2519.203	Si I	1	0.01	4.91	17
2524.108	Si I	1	0.01	4.90	18
2528.510	Si I	1	0.03	4.91	18
2532.38	Si I	86	1.90	6.77	8
2541.83	Si III	8	10.23	15.09	18
2631.28	Si I	83	1.90	6.59	12
2790.768	Mg II	3	4.40	8.83	4
2795.523	Mg II	1	0.00	4.41	22
2797.989	Mg II	3	4.41	8.83	9
2802.698	Mg II	1	0.00	4.40	21
2816.189	Al II	7	7.39	11.77	10
2852.120	Mg I	1	0.00	4.33	2
2881.595	Si I	43	0.78	5.06	24
2904.29	Si II	17	9.79	14.04	6
2905.70	Si II	17	9.80	14.04	10
2936.96	Mg II	2	4.41	8.62	1
2987.65	Si I	1	0.78	4.91	16
3072.971	Ti II	5	0.00	4.02	0
3075.225	Ti II	5	0.01	4.02	0
3078.645	Ti II	5	0.03	4.04	1
3082.159	Al I	3	0.00	4.00	12
3086.225	Si III	1	17.63	21.63	9
3088.027	Ti II	5	0.05	4.05	3

Wavelength (Å)	Element	Multiplet[5,6] Number	Excitation Potential Low	Excitation Potential High	Relative Intensity (visual)
3092.716	Al I	3	0.01	4.00	17
3092.843	Al I	3	0.01	4.00	
3096.786	Si III	1	17.64	21.62	1
3129.76	Zr II	5	0.04	3.98	2
3129.16	Zr II	23	0.52	4.47	
3129.44	O II	14	25.53	29.47	
3149.56	Si IV	2	26.95	30.86	6
3165.72	Si IV	2	26.97	30.86	
3165.98	Zr II	5	0.16	4.06	12
3166.29	Zr II	48	0.80	4.70	
3179.34	B II	Uncl.			1
3179.332	Ca II	4	3.14	7.02	
3203.89	Si II	7	10.02	13.87	6
3210.04	Si II	7	10.03	13.87	12
3210.52	Si III	Uncl.			
3234.517	Ti II	2	0.05	3.86	6
3234.00	Si III	6	21.62	25.44	
3236.573	Ti II	2	0.03	3.84	4
3239.037	Ti II	2	0.01	3.82	2
3241.984	Ti II	2	0.00	3.81	3
3241.67	Si III	6	21.63	25.44	
3247.540	Cu I	1	0.00	3.80	20
3261.596	Ti II	66	1.23	5.01	2
3261.596	Ti II	89	1.88	5.67	
3265.46	O III	8	36.32	40.10	1
3273.957	Cu I	1	0.00	3.77	19
3279.26	Zr II	3	0.09	3.86	4
3282.329	Ti II	66	1.22	4.98	1
3284.72	Zr II	4	0.00	3.76	1
3302.34	Na I	2	0.00	3.74	6
3302.94	Na I	2	0.00	3.74	
3322.936	Ti II	7	0.15	3.86	4
3323.61	B II	Uncl.			
3341.875	Ti II	16	0.57	4.26	6
3343.770	Ti II	7	0.15	3.84	2
3349.399	Ti II	1	0.05	3.73	10
3361.213	Ti II	1	0.03	3.70	7

Wavelength (Å)	Element	Multiplet[5,6] Number	Excitation Potential Low	Excitation Potential High	Relative Intensity (visual)
3372.800	Ti II	1	0.01	3.67	5
3383.761	Ti II	1	0.00	3.65	4
3388.29	Zr II	2	0.00	3.64	3
3388.87	Zr II	74	0.97	4.61	
3391.96	Zr II	1	0.16	3.80	9
3410.26	Zr II	11	0.41	4.03	1
3430.53	Zr II	11	0.46	4.06	1
3438.23	Zr II	1	0.09	3.68	8
3451.41	B II	1	9.06	12.64	24
3452.28	B II	Uncl.			
3479.39	Zr II	46	0.71	4.26	2
3481.14	Zr II	46	0.80	4.34	3
3483.54	Zr II	33	0.75	4.30	1
3496.18	Zr II	1	0.04	3.57	7
3505.67	Zr II	1	0.16	3.68	
3505.47	Zr II	90	1.53	5.05	3
3504.890	Ti II	88	1.88	5.40	
3510.840	Ti II	88	1.88	5.40	1
3535.40	Ti II	98	2.05	5.54	1
3542.65	Zr II	113	1.75	5.24	1
3551.94	Zr II	1	0.09	3.57	2
3556.61	Zr II	9	0.46	3.93	3
3572.47	Zr II	1	0.00	3.45	5
3576.88	Zr II	9	0.41	3.86	2
3586.9	Al II	7(9)*	11.80	15.24	15
3590.46	Si III	7	21.79	25.22	4
3596.048	Ti II	15	0.60	4.04	1
3601.623	Al III	1	14.31	17.74	5
3612.352	Al III	1	14.31	17.73	3
3614.79	Zr II	9	0.36	3.77	1
3685.192	Ti II	14	0.60	3.95	4
3685.192	Ti II	14	0.57	3.92	
3698.17	Zr II	71	1.01	4.34	2
3713.103	Al III	4	17.74	21.07	1

* 9 lines contribute to this multiplet.

Wavelength (Å)	Element	Multiplet[5,6] Number	Excitation Potential Low	Excitation Potential High	Relative Intensity (visual)
3727.33	O II	3	22.88	26.19	1
3727.72	Zr II	112	1.74	5.05	
3736.901	Ca II	3	3.14	6.44	1
3749.49	O II	3	22.90	26.19	2
3751.60	Zr II	71	0.97	4.26	1
3759.291	Ti II	13	0.60	3.89	4
3759.87	O III	2	33.04	36.32	
3761.320	Ti II	13	0.57	3.85	3
3791.41	Si III	5	21.62	24.88	2
3791.26	O III	2	33.04	36.29	
3796.11	Si III	5	21.62	24.88	4
3806.56	Si III	5	21.63	24.88	7
3836.76	Zr II	16	0.56	3.77	2
3853.657	Si II	1	6.83	10.03	9
3856.021	Si II	1	6.83	10.03	24
3862.592	Si II	1	6.83	10.02	21
3881.97	Zr II	134	2.40	5.58	1
3882.197	O II	12	25.55	28.73	
3905.527	Si I	3	1.90	5.06	22
3911.960	O II	17	25.55	28.71	1
3918.997	C II	4	16.26	19.41	1
3920.677	C II	4	16.26	19.41	1
3924.44	Si III	Uncl.			1
3933.664	Ca II	1	0.00	3.14	18
3944.009	Al I	1	0.00	3.13	14
3961.523	Al I	1	0.01	3.13	16
3968.470	Ca II	1	0.00	3.11	14
3970.074	H_ε	1	10.15	13.26	1W
3973.263	O II	6	23.34	26.45	1
3991.14	Zr II	30	0.75	3.85	2
3998.98	Zr II	16	0.56	3.64	1
3998.635	Ti I	12	0.05	3.13	
4062.90	O II	50	28.58	31.62	1
4069.897	O II	10	25.53	28.56	3
4069.636	O II	10	25.52	28.56	

Wavelength (Å)	Element	Multiplet[5,6] Number	Excitation Potential Low	High	Relative Intensity (visual)
4072.164	O II	10	25.54	28.57	3
4076.00	C II	36	24.27	27.30	6
4075.868	O II	10	25.55	28.58	
4088.863	Si IV	1	23.95	26.97	8
4097.260	O II	20,48	25.72	28.73	2
4096.543	O II	21	25.73	28.74	
4101.737	H_δ	1	10.15	13.16	3W
4102.926	Si I	2	1.90	4.91	2
4116.104	Si IV	1	23.95	26.95	3
4121.95	B II	2	18.60	21.59	5
4128.053	Si II	3	9.79	12.78	23
4130.884	Si II	3	9.80	12.78	24
4149.22	Zr II	41	0.80	3.77	2
4149.897	Al III	5	20.47	23.44	2
4150.138	Al III	5	20.47	23.44	
4189.788	O II	36	28.24	31.18	2
4267.27	C II	6	17.97	20.86	6
4267.02	C II	6	17.97	20.86	
4275.52	O II	67	28.73	31.62	1
4340.468	H_γ	1	10.15	13.00	10W
4349.426	O II	2	22.90	25.74	2
4347.425	O II	16	25.55	28.39	
4366.896	O II	2	22.90	25.73	2
4414.909	O II	5	23.34	26.14	3
4416.975	O II	5	23.32	26.11	
4479.966	Al III	8	20.69	23.45	2
4479.891	Al III	8	20.69	23.45	
4512.535	Al III	3	17.73	20.47	1
4529.176	Al III	3	17.74	20.47	2
4552.654	Si III	2	18.92	21.63	4
4567.872	Si III	2	18.92	21.62	2
4641.811	O II	1	22.88	25.54	1
4649.139	O II	1	22.90	25.55	3
4661.635	O II	1	22.88	25.53	1
4861.332	H_β	1	10.15	12.69	15

Wavelength (Å)	Element	Multiplet[5,6] Number	Excitation Potential Low	High	Relative Intensity (visual)
5041.063	Si II	5	10.02	12.47	15
5056.020	Si II	5	10.03	12.47	20
5105.541	Cu I	2	1.38	3.80	1
5688.205	Na I	6	2.10	4.27	1
5682.633	Na I	6	2.09	4.27	
5889.953	Na I	1	0.00	2.10	18
5895.923	Na I	1	0.00	2.09	16
5957.612	Si II	4	10.02	12.09	4
5978.970	Si II	4	10.03	12.09	10
6154.225	Na I	5	2.09	4.10	3
6160.747	Na I	5	2.10	4.10	
6243.36	Al II	10	13.02	15.00	1
6347.091	Si II	2	8.09	10.03	24
6371.359	Si II	2	8.09	10.02	22
6562.817	H_α	1	10.15	12.04	25

APPENDIX I

Streak Photography

The general arrangement of the streak camera is shown in Fig. I-1. The object, O, to be photographed is reflected off the rotating mirror, M, on to the 35 mm film strip, F.

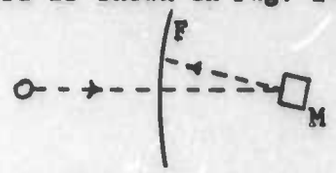

Fig. I-1

The developed film strip pres entation is shown in Fig. I-2.

The velocity of the exposure on the film strip may be expressed as:

$$v_f = 2\pi fR \qquad \text{(I-1)}$$

where f = frequency of rotating mirror

R = radius of curvature of the streak camera film holder.

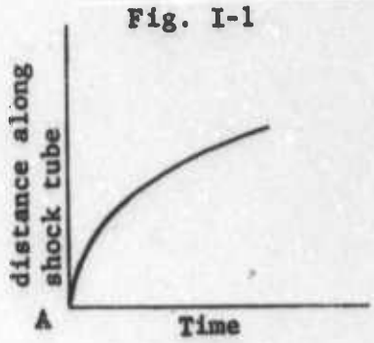

Fig. I-2

If the velocity of the luminous shock front, v, is desired at point A shown in Fig. I-2, a tangent (i.e. slope or velocity) at that point may be constructed as shown in Fig. I-3. The right triangle shown has sides v_f and mv where m is the magnification of the streak photograph and v is the desired velocity of the luminous shock front at point A. Therefore:

$$v = \frac{1}{m} v_f \tan \theta \qquad \text{(I-2)}$$

Combining I-1 and I-2,

$$v = \frac{2\pi fR}{m} \tan \theta \qquad \text{(I-3)}$$

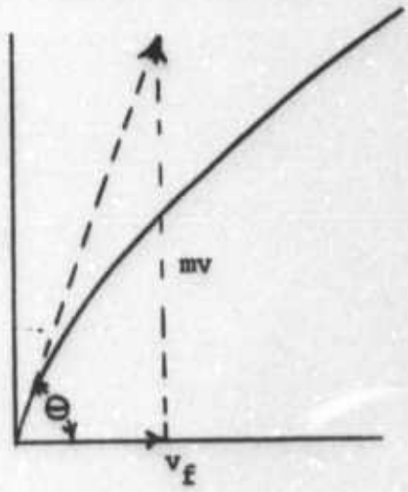

Fig. I-3

R was determined by direct measurement on the streak camera. The quantities θ and m were determined from the film strip, whereby f was obtained through the use of a counter and timer connected to the axis of the rotating mirror.

APPENDIX II

Spectroscopic Techniques

It was necessary to make a number of calibrations for the experimental equipment. Since the Gaertner L 254 spectrograph and associated equipment will be available at the Postgraduate School for further research work, the results of the calibrations made are listed below for future reference.

A. Slit width calibration

The jaws of the slit were checked and found to be parallel and in excellent conditon. The various slit width settings were measured and plotted. Fig. II-1 is a curve of slit width setting versus the measured slit width.

B. Timer Calibration

The following timer settings were determined:

Dial Setting (sec)	Measured Time (sec)
0.5	0.5
1.0	1.0
1.6	1.5
2.0	2.4
4.0	4.9

C. Step Filter Calibration

The source of the transmission values for the step filter was unknown. Measurements made showed considerable variation with the rated transmission values provided.

Step number, n	Rated I_n/I_o	Measured I_n/I_o
1	1.0	1.0
2	0.627	0.406
3	0.390	0.244
4	0.250	0.147
5	0.156	0.065
6	0.100	0.030
7	0.064	0.012

D. Other Calibrations

The spectrograph was cleaned, aligned, and focused by Aerospace Corporation after receipt of the instrument from NOTS, China Lake, California. The Standard Lamp and associated equipment was similarly calibrated by Aerospace Corporation prior to experimental measurements.

The measurement of radiant energy spectroscopically is a very difficult and sensitive problem. There are many factors involved, which, if not properly compensated for, will lead to meaningless values. In general, the recommended methods of Sawyer[2]; Brode[3]; and Harrison, Lord and Loofbourow[4] were followed in the intensity determinations.

Particular attention was given to the following items:

1. Pre-measurement checks
2. Plate exposure
3. Plate developing
4. Plate calibration.

Pre-measurement checks included careful warming and insertion of the spectroscopic plate, check of spectrograph alignment, focus and optical set-up, and the complete darkening of the room prior to measurement.

Plate exposures of the shock tube firing and the Standard Lamp were taken through identical optical set-ups with the exception of the Standard Lamp window which necessitated a separate compensation in the data reduction calculations. The exposures were taken over a short time interval to reduce the affect of ambient temperature and pressure variations on the spectrograph.

Temperature and time criteria were closely adhered to in the developing and processing of the plates. The chemicals used were freshly made, and constant agitation was also employed.

The densitometer used in plate calibrations was carefully checked to insure that it was fully warmed and steadied out prior to use. After each densitometer run was made, a check was immediately made to insure that drift has not occurred during the run.

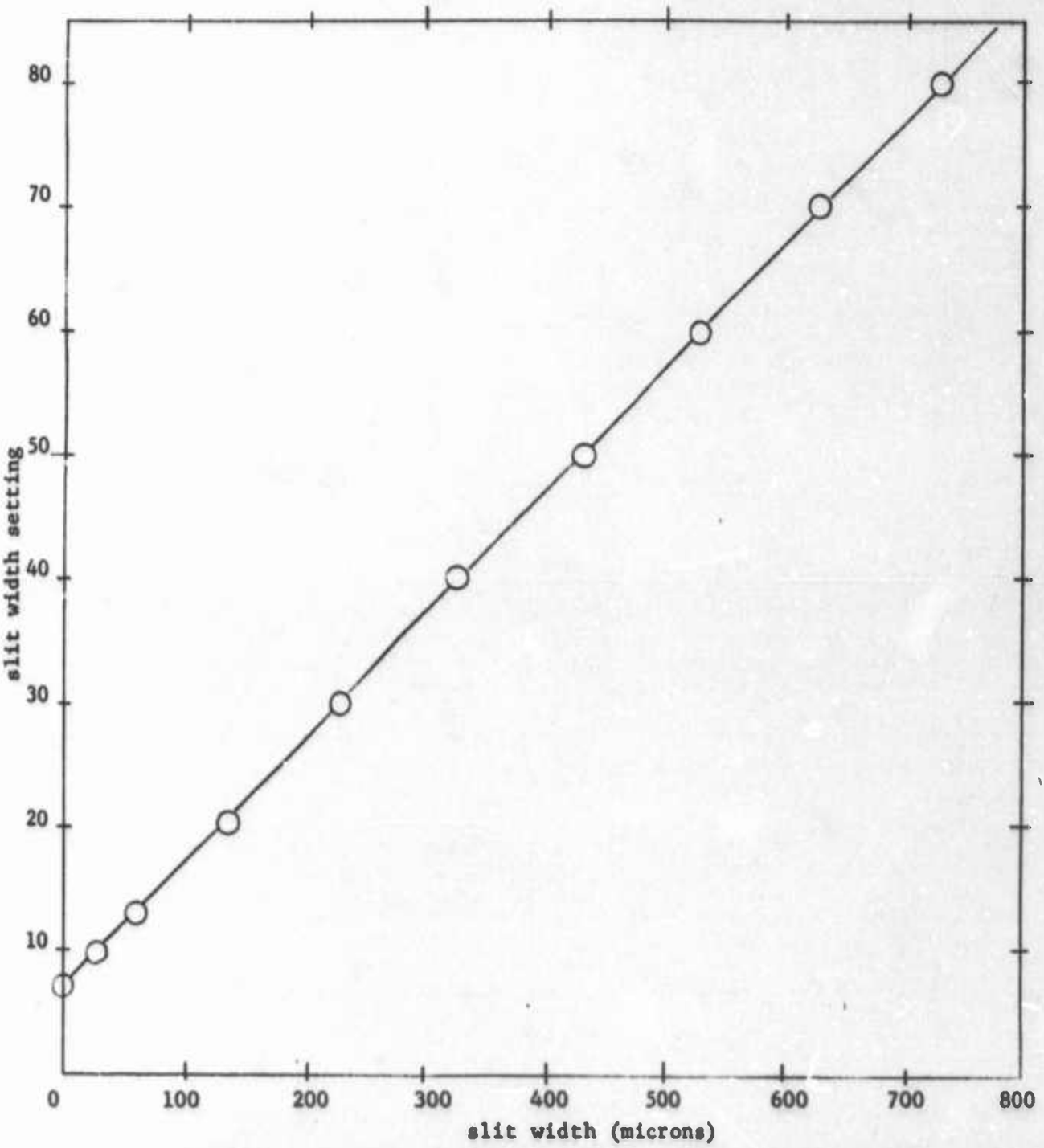

Fig. II-1. Slit Width Calibration

REFERENCES

1. V. Josephson and R.W. Hales, Parametric Study of the Conical Shock Tube, Phys. Fluids, 4, pp. 373, 1960.

2. R.A. Sawyer, Experimental Spectroscopy, Prentice-Hall, Inc., New York 1951.

3. W.R. Brode, Chemical Spectroscopy, John Wiley & Sons, Inc., New York 1958.

4. G.R. Harrison, R.C. Lord, and J.R. Loofbourow, Practical Spectroscopy, Prentice-Hall, Inc., 1948.

5. C.E. Moore, A Multiplet Table of Astrophysical Interest, Tech. Note 36, National Bureau of Standards, 1959.

6. C.E. Moore, An Ultraviolet Multiplet Table, Circular 488, Section 1, National Bureau of Standards, 1950.

7. A.D. Code, Stellar Energy Distribution, (in J.L. Greenstein, Stellar Atmospheres, pp. 50, University of Chicago Press, 1960).

8. W. Lochte-Holtgreven, Production and Measurement of High Temperatures, Reports on Progress in Physics, XXI, pp. 312, 1958.

9. D.R. Inglis and E. Teller, Ionic Depression of Series Limits in One-Electron Spectra, Astophys. J., 90, pp. 439, 1939.

10. H.R. Griem, A.C. Kolb, and K.Y. Shen, Stark Broadening of Hydrogen Lines in Plasma, U.S. Naval Research Laboratory, Washington D.C., 1960.

11. G.H. Dieke, Spectroscopy of Combustion, (in R.W. Ladenburg, et.al., Physical Measurements in Gas Dynamics and Combustion, pp. 467, Princeton University Press, 1954).

12. L.M. Branscomb, The Program at the National Bureau of Standards, (in P.J. Dickerman, Optical Spectrometric Measurements of High Temperature, pp. 235, University of Chicago Press, 1961).

13. W.J. Pearce, Plasma-Jet Temperature Measurement, (in Dickerman, op. cit., pp. 125).

14. P.J. Dickerman and J.C. Morris, Experimental Studies of the Temperature in a Field-Free Plasma, (in Dickerman, op. cit., pp. 170).

15. H. Margenau and M. Lewis, Structure of Spectral Lines From Plasmas, Revs. Modern Phys., 31, pp. 569, Jul 1959.

16. E.A. McLean, C.E. Faneuff, A.C. Kolb and H.R. Griem, Spectroscopic Study of Helium Plasmas Produced by Magnetically Driven Shock Waves, Phys. of Fluids, 3, pp. 843, 1960.

17. R.M. Head, The Emission Spectra Behind Ionizing Shock Waves in Hydrogen, Aerospace Corp., 1962.

18. C.W. Allen, Astrophysical Quantities, University of London, 1955, (Allen points out the need for f-values and the discrepancies between theoretical and observed values).

19. L. Spitzer, Physics of Ionized Gases, Interscience Publishers, Inc., 1956.

20. K.H. Böhm, Basic Theory of Line Formation, (in Greenstein, op. cit., pp. 88).